Available online at www.sciencedirect.com

ScienceDirect

Journal of Magnesium and Alloys 10 (2022) 1086–1095

www.elsevier.com/locate/jma

Full Length Article

Microstructure, mechanical properties, and corrosion resistance of an explosively welded Mg–Al composite

Mustafa Acarer[a,*], Bilge Demir[b], Burak Dikici[c], Emin Salur[a]

[a] Department of Metallurgical and Materials Engineering, Technology Faculty, Selcuk University, Konya 42075, Turkey
[b] Department of Mechanical Engineering, Karabuk University, Karabuk 78100, Turkey
[c] Department of Metallurgical and Materials Engineering, Atatürk University, Erzurum 25240, Turkey

Received 17 May 2021; received in revised form 16 July 2021; accepted 3 August 2021
Available online 6 September 2021

Abstract

In this study, an attempt was made to manufacture an AZ31–Al5005 laminated composite by explosive welding. A mixture of ammonium nitrate (90%), fuel oil (5%), and TNT (5%) was used as the explosive. The detonation velocity of the explosive material was approximately 3100 m•s^{-1}. The microstructure and mechanical and corrosion properties of the joint were comparatively investigated. Microstructural characterisation of the joint was conducted by optical microscopy (OM), scanning electron microscopy with energy-dispersive spectroscopy (SEM-EDS), high-resolution transmission electron microscopy (HR-TEM), and X-ray diffraction (XRD). The mechanical properties were determined using micro-Vickers hardness, tensile, and Charpy impact tests. In addition, electrochemical tests were conducted on the AZ31–Al5005 laminated composite and the individual components to determine their corrosion resistance. The corrosion behaviours of the structures were determined in a 3.5% NaCl solution at room temperature using potentiodynamic scanning (PDS). The metallurgical structure and mechanical properties of the joints were within the acceptable limits.

Keywords: AZ31; Al5005 explosive welding; Microstructure; Mechanical properties; Corrosion resistance.

1. Introduction

Explosive cladding or welding is a solid-state welding process used to join a wide variety of similar and dissimilar metals and alloys with different physical and mechanical properties. Although this process is classified as a cold technique, some local melted zones may form at the interface owing to the high-pressure dynamics generated by the explosives [1–3]. The unique feature of this welding method is that it can join metals with different melting temperatures. In addition, this method can be used to produce laminated metallic composites with different properties using very different metal combinations. Therefore, the use of a combination of metal sheets and an explosive welding method is considered to be an important process for joining metals [4].

Numerous attempts have been made to reveal the effects of explosive welding parameters [2] on the microstructure and mechanical properties of explosively welded bimetals, such as stainless steel-carbon steel [5–7], aluminium–steel [3,8,9], and copper-steel [10]. However, studies on the explosive welding of magnesium to other metals are limited. Ghaderi et al. [11] attempted to determine the optimum welding conditions for the explosive welding of aluminium to magnesium. Habib et al. [12] reported the explosive welding of titanium to magnesium using underwater shockwaves. The effects of the welding parameters on the weld integrity of explosively welded magnesium–aluminium joints were discussed in another study by Ghaderi et al. [13]. The reason for the limited number of studies is probably the poor ductility and formability of magnesium alloys resulting from their hexagonal close-packed (HCP) crystal structure. In explosive welding, the welded metals must have at least 5% elongation. Therefore, the weldability of magnesium alloys by explosions is limited by their mechanical properties [14].

* Corresponding author.
E-mail address: macarer@selcuk.edu.tr (M. Acarer).

https://doi.org/10.1016/j.jma.2021.08.009

Table 1
The chemical compositions of AZ31 and Al5005 sheets.

Element (wt%)	Al	Mg	Zn	Mn	Fe
AZ31	2.5	bal.	1.0	0.2	–
Al5005	bal.	0.9	0.2	0.1	0.5

There are some studies [15–17] on the corrosion properties of explosively welded laminated composites. Kaya [15] investigated the corrosion resistance of aluminium clad to ship steel plates by explosive welding. The neutral salt spray test results showed that cladding aluminium on top of ship steel using explosive welding protected the ship steel against corrosion in a seawater environment. In another study [16], the corrosion behaviours of steel–aluminium composite structures produced via explosive welding were evaluated using immersion tests in NaCl solutions. After the corrosion tests, the metallographic observations revealed that the molten zones during the explosive welding preferentially acted as corrosion initiation points in the joint, and metal losses were mainly observed in these zones. The study showed that corrosion degradation does not depend on the explosive conditions owing to the complete erosion of the molten zones. It has also been reported that an area susceptible to intercrystalline corrosion can form owing to the heat generated and rapid diffusion in the weld zone (or non-diffusion mass transport) during explosive cladding [17].

Similar to studies on the explosive welding of Mg alloys, studies on the corrosion properties of bimetals produced by explosive welding are limited. However, detailed studies are needed to understand the joining and corrosion damage mechanisms of bimetals with different crystal structures, such as hexagonal close-packed (HCP) and face-centred cubic (FCC) phases, produced by explosive welding. Therefore, the microstructure and interface characteristics, mechanical properties, and corrosion resistance of explosively welded AZ31–Al5005 alloys were investigated in this study.

2. Experimental procedure

AZ31 magnesium alloy sheet was used as the flyer metal, and 5005 aluminium alloy sheet was used as the parent metal to produce laminated composites in this study. The chemical compositions of the AZ31 and Al5005 alloys are listed in Table 1.

The dimensions of the AZ31 and Al5005 sheets were 150 × 150 × 4 mm^3 and 150 × 150 × 1.5 mm^3, respectively. Rubber layers were used as the buffer zone between both the AZ31 and explosive and the Al5005 and anvil to minimise the deformation of the AZ31 and Al5005 sheets during the explosion. A mixture of ammonium nitrite (90%), fuel oil (5%), and TNT (5%) was used as the explosive. The detonation velocity of the explosive material was approximately 3000–3200 $m \cdot s^{-1}$.

The cross section of the joint was ground with increasingly fine sandpaper to remove the cutting traces formed on it. Then, the surfaces were polished with 1 μm diamond paste and ultrasonically cleaned with ethanol. AZ31 was etched in

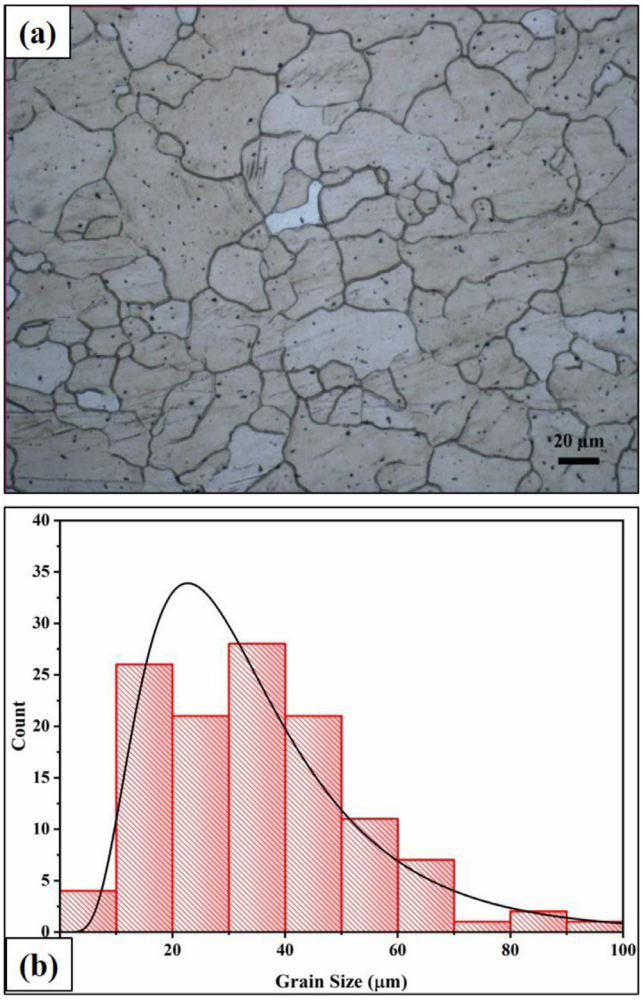

Fig. 1. The microstructure of AZ31 magnesium alloy: **(a)** optical micrograph, and **(b)** histogram of grain size distribution.

a solution containing 10 ml acetic acid, 5 g picric acid, 10 ml ethanol, and 75 ml distilled water. The microstructural characterisation of the joint was conducted by optical microscopy (OM, NIKON Epiphot 200), scanning electron microscopy with energy-dispersive spectroscopy (SEM–EDS, Jeol JSM 5600), high-resolution transmission electron microscopy (HR-TEM, JEOL JEM-2100), and X-ray diffraction (XRD).

The mechanical properties were determined using a microhardness tester (LECO DM-400) under a 10 gf load for 15 s. The average values from across the weld interfaces were reported. Tensile and impact tests were performed to determine the strength/elongation and toughness of the laminated composite structure, respectively. The toughness of the AZ31–Al5005 composite was measured by Charpy V-notch tests at +25, 0, −25, and −50 °C using a DEVOTRANS test machine with a 50 *J* hammer.

The corrosion behaviours of the joints and their base metals were determined using the potentiodynamic scanning (PDS) technique at room temperature. The changes in the potential (*E*) vs. current (*I*) of the samples were recorded using a potentiostat unit (Gamry, PCI14/750) in a 3.5% NaCl so-

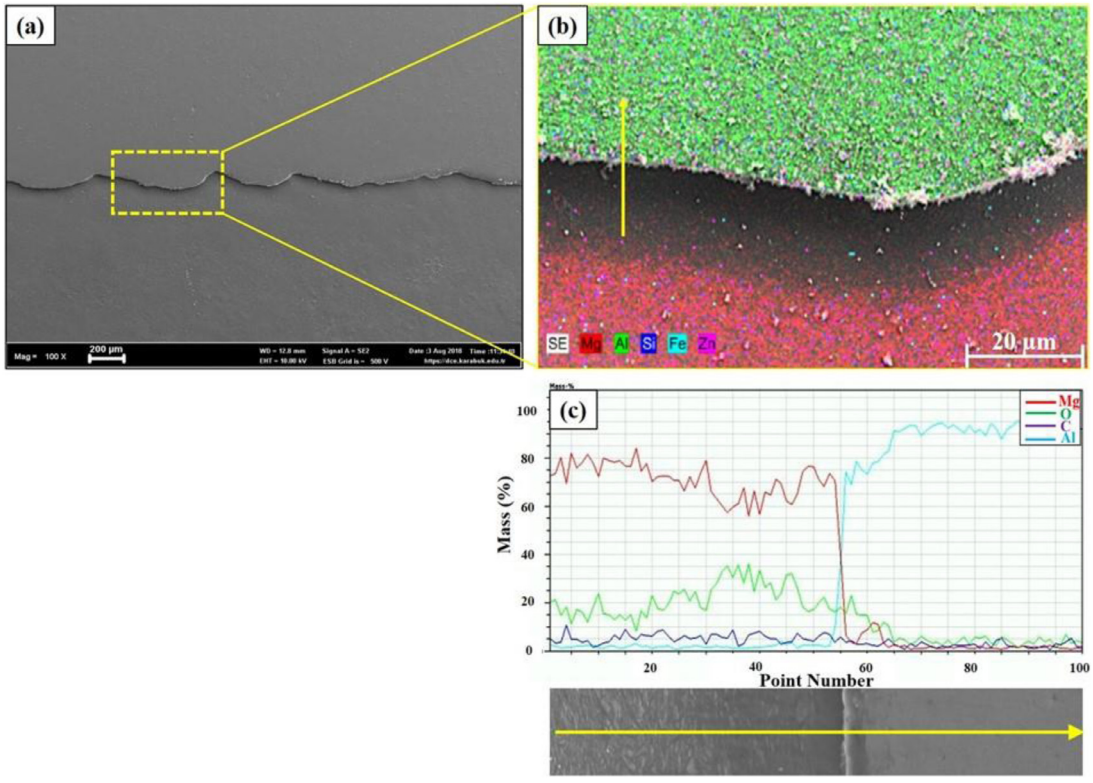

Fig. 2. **(a)** Wavy interface, **(b)** mapping and **(c)** EDS line analysis of the AZ31–Al5005 composite.

lution. Ag/AgCl and Pt wire were used as the reference and counter electrodes, respectively, during the tests. The scan rate of the PDS measurements was 1 $mV \bullet s^{-1}$. The sample area was approximately 0.5 cm^2, and all data were normalised to the surface area. Both the fractured and corroded surfaces were investigated by SEM.

3. Results and discussion

3.1. Microstructure

The microstructure of the AZ31 magnesium alloy (before the explosive welding process) used as a flyer metal is shown in Fig. 1. The AZ31 Mg alloy consisted of almost equiaxed α-Mg grains (Fig. 1b).

The AZ31–Al5005 laminate composite was produced by an explosive welding technique. Even when precautions were taken (such as annealing before the welding process and using a buffer zone during the explosion), cracks were observed locally on the Mg side because the number of slip systems was insufficient to allow deformation of the Mg sheet under the shock wave generated during explosive welding.

The microstructure of the welding interface and elemental mapping and line analysis of the AZ31–Al5005 composite produced by explosive welding are shown in Fig. 2a–c, respectively. A wavy interface was observed in the explosively welded AZ31–Al5005 composite (Fig. 2a).

The morphology of the interface was wavy (Fig. 2a) because the explosive loading was sufficient to produce a wavy interface. Straight and wavy interfaces can be formed between explosively welded materials. Increasing the explosive loading increases the impact energy of the flyer plate, which causes a transition from a straight to a wavy interface [5]. To further analyse the wavy interface formed by the explosion, EDS mapping analyses were performed primarily for the welding interface region, as illustrated in Fig. 3. Although almost the entire interface showed a sharp transition (Figs. 3 and 4), partially molten regions (Fig. 5) were also observed. The presence of both Mg and Al in the crystal structures at the interface indicates a sharp transition at the junction interface. Fig. 4 shows a TEM image and diffraction patterns of the Mg and Al sides of the joining interface shown in Fig. 3a. Fig. 4a shows a representative HR-TEM micrograph of the AZ31–Al5005 interface transition zone. As shown in the upper area in Fig. 4a, the interplanar spacing was measured to be 0.2340 ± 0.010 nm, which matches the (11–21) reflection of Mg. The lattice spacing calculated from the upper region was 0.2032 ± 0.015 nm, which corresponds to the (200) plane of Al. Nanometric grain boundaries were observed because of the rearrangement of crystallites in different orientations during the explosion. Furthermore, selected area electron diffraction (SAED) indexing was conducted for qualitative phase analysis of the elements in the transition zone, as shown in Fig. 4b. The four rings, consisting of continuous diffraction spots, correspond to Mg (−1121), Al (200), Mg (−1120), and Al (311), respectively, in the outward radial direction.

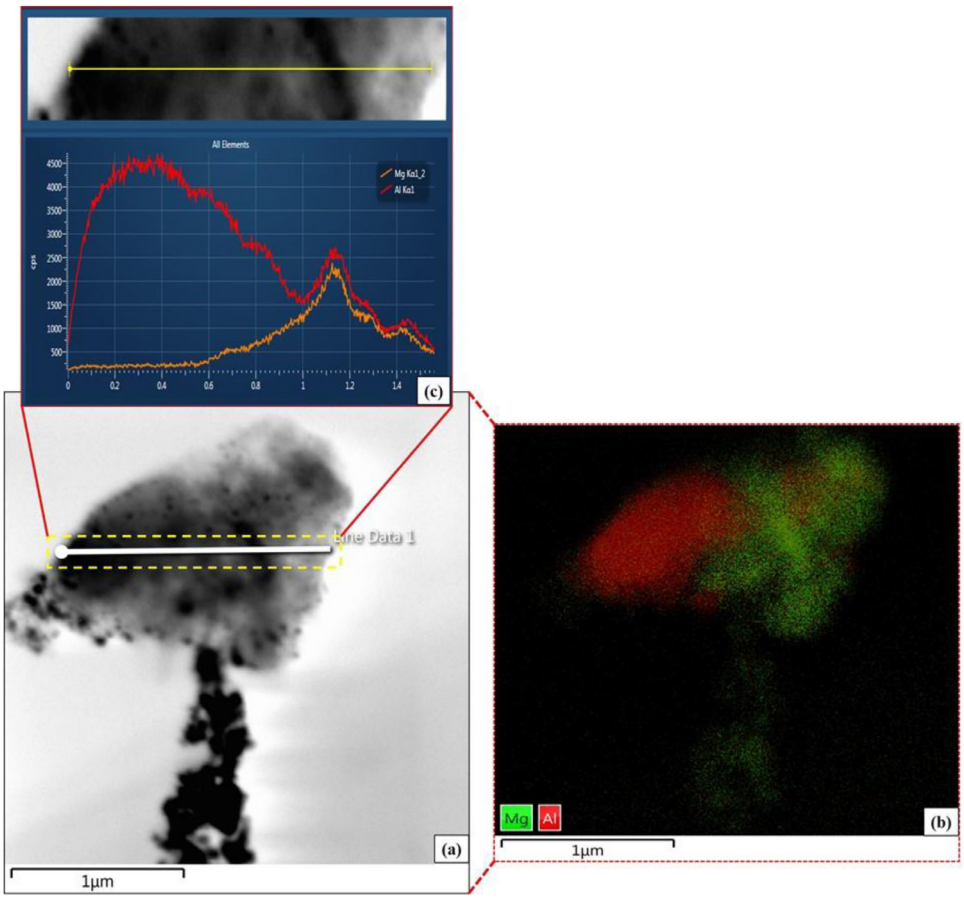

Fig. 3. **(a)** TEM image of welding interface in the AZ31–Al5005 composite, and **(b,c)** its elemental mapping analyses.

Local melted regions in the interface probably formed via melting and solidification during explosive welding, in which the kinetic energy between AZ31 and Al5005 during the explosion produced the required melting temperature. Ghaderi et al. [11] reported that despite the high temperatures generated at the interface, the high velocity of the process and immediate heat transfer to the bulk of the materials creates conditions that are insufficient for melting or diffusion. However, they also observed that the eddy regions in which metallurgical changes occurred owing to the re-entrant jet caused localised temperature increases and melting. The compositional changes may have been caused by melting. Zhang et al. [10] observed a diffusion layer in a AZ31B and Al6061 welding interface. They attributed this phenomenon to metallurgical bonding of the interface in the AZ31B/Al6061 composite plates. In this study, intermetallic structures were also observed (Fig. 6a and b), which were identified as Mg_3Al_2 and Mg_2Al_3 via SAED. As shown in the upper side of Fig. 6a, the interplanar spacing was measured to be 0.2774 ± 0.010 nm, which is consistent with the (100) reflection of Mg. The lattice spacing calculated from the lower region in Fig. 6a was 0.2290 ± 0.015 nm, which corresponds to the interplanar spacing of the (1222) plane of Mg_2Al_3. These outcomes agree to a great extent with the XRD results shown in Fig. 7. A closer examination of the 40°–60° region of the XRD data showed that traces of some intermetallic phases were visible within the resolution limit of the XRD analysis. Therefore, the XRD results, which are in good agreement with the HRTEM and SAED indexing results, clearly show the formation of intermetallic phases generated by the combined effect of the melting and solidification processes. Jonnard et al. [18], Mofid et al. [19], and Wachowski et al. [20] reported the formation of $Mg_{17}Al_{12}$, Mg_3Al_2, and Mg_2Al_3 intermetallic phase in Mg–Al alloys and Mg–Al couples. It is thought that the formation of these intermetallic structures is due to melting and subsequent solidification. In the TEM investigation, no amorphous structures, which can form owing to the high cooling rates (105–106 °C·s^{-1}) in the melting–solidification process, were observed. Paul et al. [21] observed an amorphous structure in carbon or stainless steel/Zr, carbon steel/Ti, and stainless steel/Ta claddings. Nishida et al. [22] reported that the interface of a Ti–stainless steel couple produced by explosive welding had a sharp transition and an amorphous structure in a locally melted–solidified zone. The HRTEM images (Figs. 4 and 6) suggest that the metals joined via metallurgical bonding during explosive welding.

Two different microstructures were observed in the AZ31 magnesium alloy side near the interface, as shown in

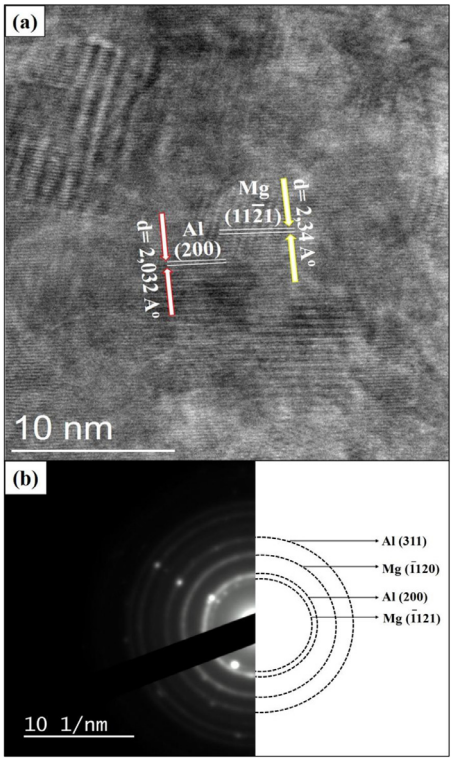

Fig. 4. **(a)** HRTEM image, and **(b)** diffraction pattern of the transition zone of AZ31–Al5005 interface.

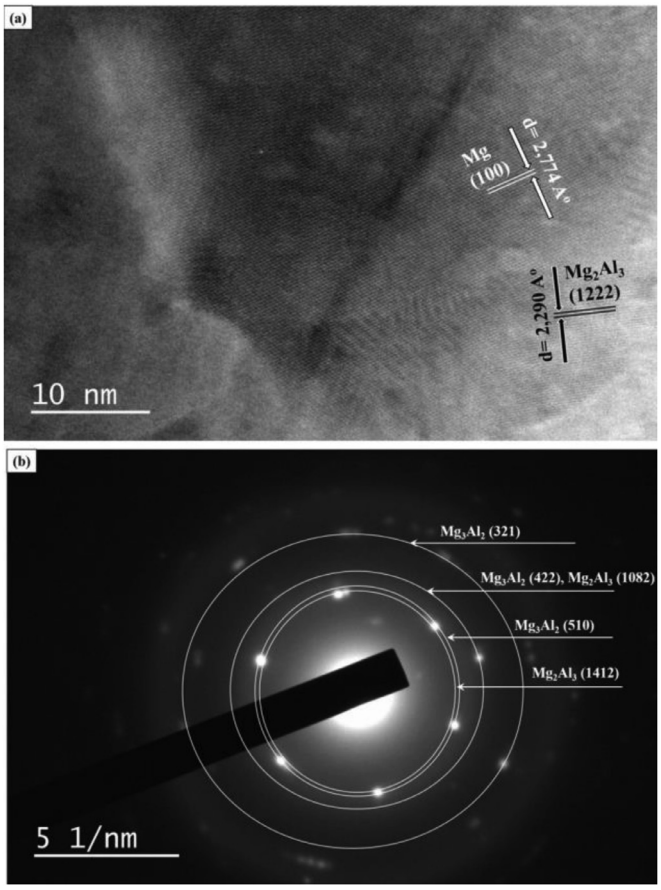

Fig. 6. The representative (a) HR-TEM image and (b) SAED pattern of the composite, showing the presence of intermetallic phases.

Fig. 8a and b. The first was adiabatic shear bands (ASB), which occurred only on the AZ31 side near the explosive welding interface and originated from the interface. The second was refined equiaxed grains, including twin structures due to deformation.

Fig. 7 shows XRD patterns of the original Mg sheet and Mg side of the AZ31–Al5005 composite. After explosive welding, the peaks shifted to lower angles owing to severe plastic deformation.

3.2. Mechanical properties

The hardness values of the as-received Al5005 and AZ31 were 50 and 78 HV, respectively. After the explosive welding process, the hardness of the AZ31 side of the composite reached 120 HV near the interface, but it gradually decreased to the original hardness away from the interface. Fig. 9 shows the change in the hardness of the AZ31–Al5005 composite with the distance from the interface. There was a similar trend in the hardness on the Al5005 side. Severe plastic deformation caused an increase in hardness near the interface. During the explosive welding process, the bottom surface of the flyer plate (the Mg sheet) collides with the upper surface of the base metal (the Al side) at a high velocity. Upon impact, the

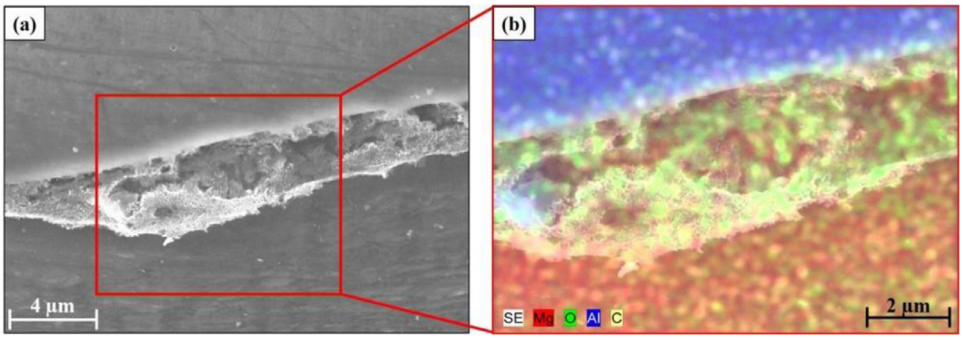

Fig. 5. **(a)** SEM image of welding interface in the AZ31–Al5005 composite, and **(b)** its elemental mapping analyses.

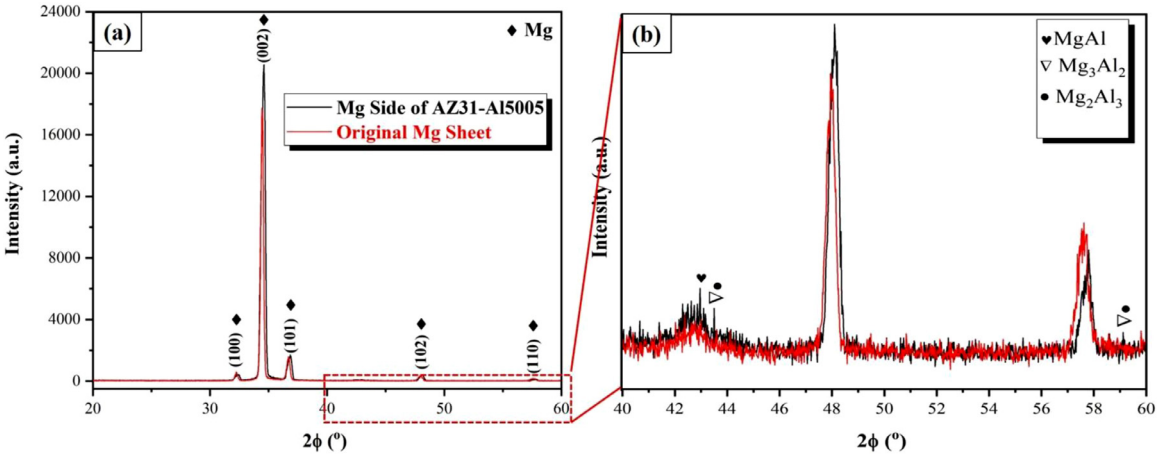

Fig. 7. **(a)** XRD pattern of original Mg sheet and Mg side of AZ31–Al5005 composite, **(b)** the peaks showing Mg_3Al ve Mg_2Al intermetallic phases.

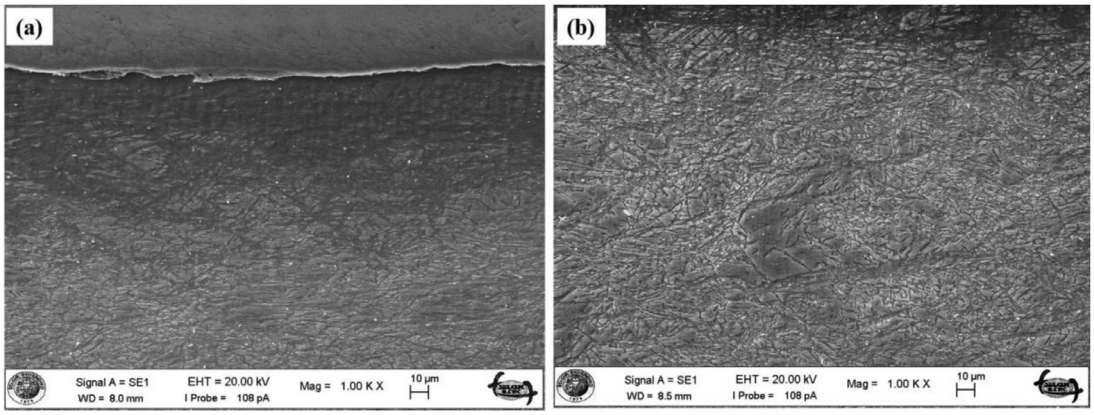

Fig. 8. **(a)** AZ31-Al5005 composite interface, and **(b)** away from the interface.

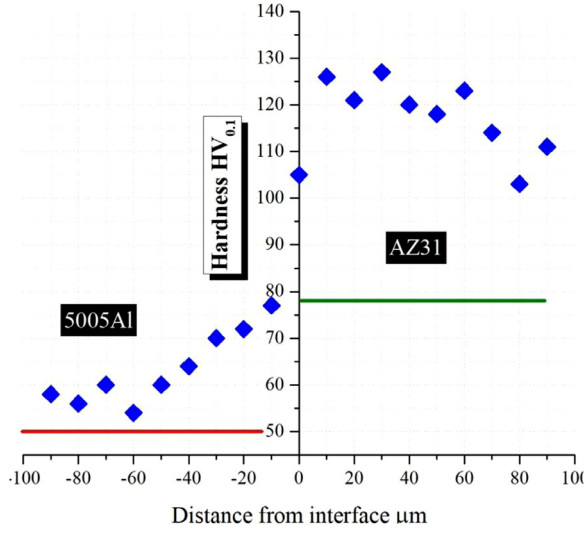

Fig. 9. The hardness of the AZ31–Al5005 composite.

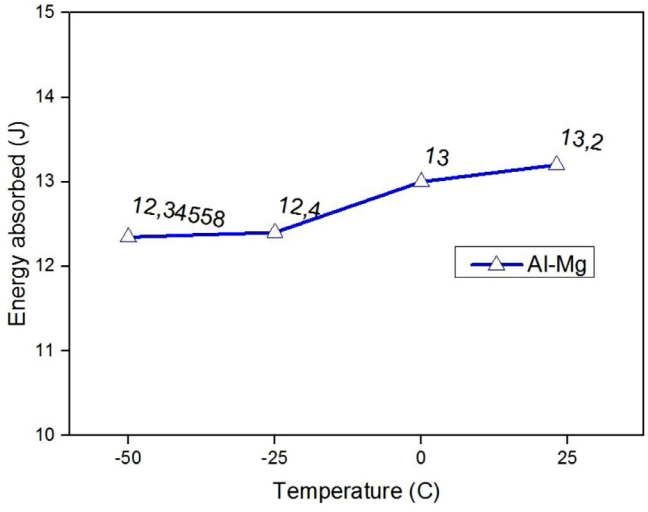

Fig. 10. Charpy *V*-notch impact test results.

kinetic energy is dissipated as heat through the surfaces of the plates or sheets. However, the increase in temperature is insufficient to recrystallise the interface of the composite, or there is insufficient time for recrystallisation to occur. Therefore, severe cold plastic deformation occurs at the interface, which is the reason for the increased hardness. However, owing to

Table 2
Tensile test results of the AZ31–Al5005 composite.

Samples	YTS, (Yield strength) (MPa)	UTS, (ultimate tensile strength) (MPa)	Strain (%)
Original AZ31	170	290	11
Original 5005 Al	110	185	4
AZ31–Al5005 composite	96	178	4

To determine the toughness of the AZ31–Al5005 composite, Charpy impact tests were conducted at +25, 0, −25, and −50 °C. The test results are shown in Fig. 10.

Table 3
Corrosion parameters of the samples calculated from PDS curves.

Samples	E_{corr} (mV)	I_{corr} ($\mu A \cdot cm^{-2}$)	Corr. Rate (mpy)
Original AZ31	−1510	111	106
Original 5005 Al	−733	0.15	0.58
AZ31–Al5005 composite	−1259	453	336

The polarisation behaviour of the AZ31–Al5005 composite was mostly similar to that of AZ31. However, the corrosion potential (E_{corr}) of the explosively welded composite structure was nobler (+250 mV) compared to that of AZ31.

the kinetic energy of the process, melted–solidified regions can form locally, as explained in the microstructure section. Therefore, the hardness near these regions can be lower than that away from the interface.

The tensile test results for the AZ31–Al5005 composite are summarised in Table 2. The results illustrate that the tensile strength and yield strength of the composite were lower than those of the individual components owing to the cracks formed during the explosive welding process. It can be seen from Table 2 that the elongation of the composite was lower than that of the AZ31 magnesium alloy and similar to that of the Al5005 alloy.

The impact energies of the AZ31–Al5005 composite varied between 12 and 13 *J* at all temperatures. Decreasing the temperature did not cause a significant change in the impact strength. For body-centred cubic (BCC) metals, decreasing the temperature causes a transition from ductile to brittle fracture. The main reason for this, and the reason it does not occur in FCC and HCP metals, is that BCC metals do not have closed-pack planes. Atomic vibrations affect the deformation (slipping) of metals, particularly at low temperatures. However, with decreasing temperature, atomic vibrations decrease, and their contribution to slip is limited. Because BCC metals do not contain close-packed atomic planes, this phenomenon is more evident. While atomic vibrations are limited at low temperatures in FCC and HCP metals, the high atomic density of these crystalline metals in the close-packed planes minimises the negative effect of low vibrations. As a result, slipping is the most prominent ductile fracture feature and plastic deformation mechanism in metals. Because the contribution of atomic vibrations to slip at low temperatures is limited, BCC metals show brittle fracture at low temperatures, while they show ductile fracture at higher temperatures [23]. In addition, the number of slip systems in HCP metals is low. Thus, ductile fracture does not occur in metals with this crystal structure.

The fracture surfaces of the Mg and Al sides of the composite showed the same characteristics at all temperatures (Fig. 11). The Al5005 surface had dimples, while there were no dimples on the Mg side. The dimples are evidence of the slip mechanism in metallic materials. Because the number of slip systems in HCP metals is very low compared to those in BCC and FCC crystalline metals, the Mg alloy fractured without significant plastic deformation.

3.3. Corrosion test results

The polarisation curves (PDS) of the original metals and explosively welded composite materials in 3.5% NaCl are presented in Fig. 12. Some important corrosion parameters calculated from these curves are listed in Table 3.

Undoubtably, aluminium and magnesium are popular because of their low densities. However, magnesium alloys are not as widely used as aluminium alloys, primarily because of their high sensitivity to corrosion, which is a major drawback that limits the widespread use of magnesium alloys in industry. However, studies on Mg alloys with high specific strength and corrosion resistance have increased in parallel with technological developments [24,25].

Magnesium alloys have very poor corrosion resistance when exposed to aggressive environments rich in chloride ions, although they are resistant to atmospheric corrosion because of the protective oxide layer that typically forms on their surface. Numerous different corrosion mechanisms can be observed for Al and Mg alloys according to their alloying components or thermomechanical history. The most common mechanisms are pitting and transgranular corrosion. However, galvanic corrosion occurs on Mg when Mg is in contact with another metal that has a nobler electrochemical potential than that of Mg [26]. Galvanic corrosion is also known as bimetallic corrosion (or dissimilar metal corrosion) and should be expected in explosively welded materials. Heavy galvanic corrosion marks were observed on the explosively welded AZ31–Al5005 structure in this study (Fig. 13).

It is well known that corrosion reactions occur at the inflection points of the PDS curves of materials, which also correspond to the E_{corr} value. In this study, the steady-state potentials of the original AZ31 and Al5005 alloys were calculated to be −1510 and −733 mV, respectively (Table 3). The large difference between the E_{corr} values of the original materials triggered galvanic corrosion in the explosively welded structure. Thus, the corrosion rate of the explosively welded structure increased owing to the high galvanic coupling between the Al5005 and AZ31 alloys (Table 3).

The corroded surfaces of the explosively welded structures at different polarisation levels are presented in Fig. 14.

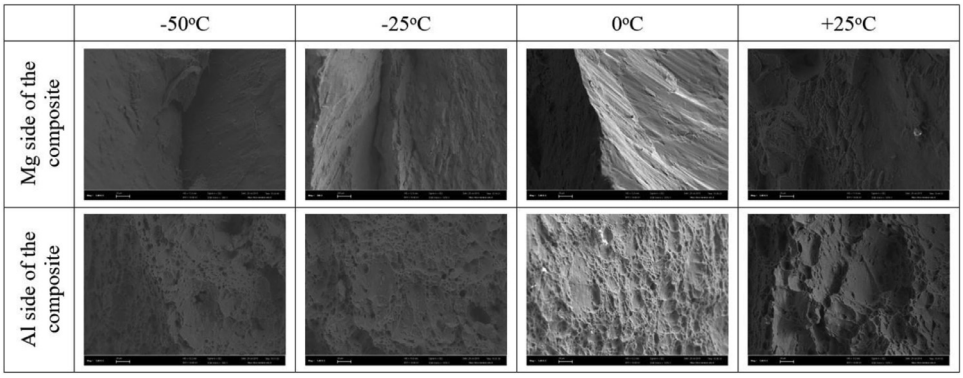

Fig. 11. The fracture surface of the AZ31–Al5005 composite.

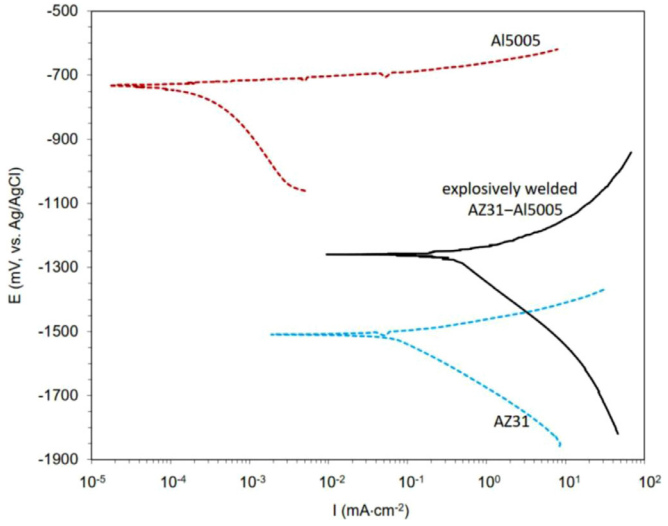

Fig. 12. Potentiodynamic scanning (PDS) curves of the samples in 3.5% NaCl.

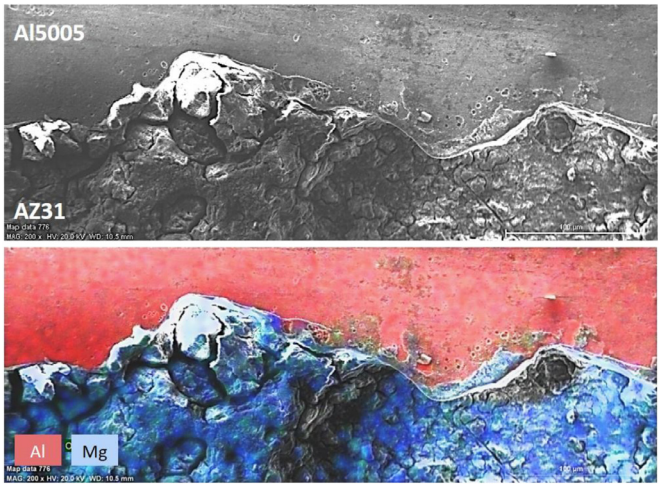

Fig. 13. Formed galvanic couplings between Al5005 and AZ31 composite structure after the corrosion tests.

Above the inflection points, the dissolution of the AZ31 matrix can be described by the Mg + $2e^{-} \rightarrow Mg^{2+}$ anodic reaction. In this stage (Fig. 14a), the AZ31 side of the explosively welded metal corroded preferentially because its electrode potential was lower than that of Al5005. Corrosion began at the Al5005/AZ31 interface (marked with an arrow in Fig. 14a). The decomposition of alloying elements in the orig-

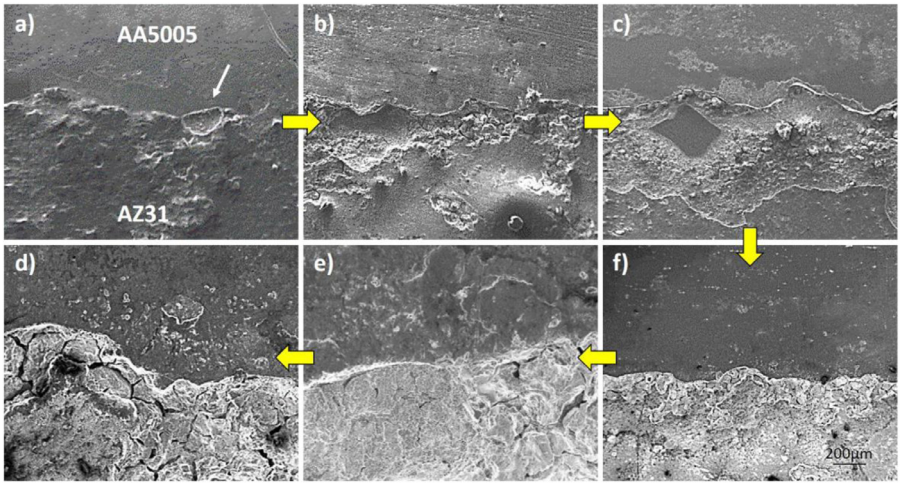

Fig. 14. The corroded surfaces of the explosively welded structure during the different polarization levels.

inal materials in these regions was inevitable because of the high temperatures generated at the interface during the welding process, which led to the formation of intermetallic phases (Figs. 7 and 8). The cathodic character of the intermetallic compounds in the interface, such as the β phase, also contributed to the corrosion behaviour [26]. These compounds increased the local cathode area in the interface. Corrosion propagated into the Mg side (Fig. 14b) with increasing polarisation level. A $Mg(OH)_2$-based oxide layer formed on AZ31. However, the magnesium oxide layer was very porous and fragile. In addition, the layer only provided partial protection owing to the occurrence of breaks and the porous structure of the layer (Fig. 14c) [27,28]. Thus, the layer was exfoliated from the surface owing to leakage of the electrolyte underneath the layer. Consequently, more in-depth oxide films formed on the AZ31 surface, as shown in Fig. 14d–f.

4. Conclusions

While different aspects of Mg and Al alloys were examined extensively in the context of the explosive welding process, the interface characteristics and corrosion properties of bimetals produced by this procedure seem to have received only cursory attention in the open literature. Therefore, the primary purpose of this study is to investigate microstructure, mechanical, and corrosion properties of joining interfaces of explosively welded AZ31 and Al5005 sheets within the framework of process-structure-property-performance correlation. For this purpose, the AZ31/Al5005 bimetal composites were successfully produced via explosive welding. The interfacial microstructure evolution, mechanical properties, and corrosion resistance of explosively welded bimetal composites were thoroughly characterized by SEM, XRD, HR-TEM, optic microscopy, Vickers hardness, tensile, Charpy impact, and corrosion tests. The key findings and the concluded remarks could be summarized as follows.

- Explosive welding has been advanced with various applications in the manufacturing industry. The process has found chiefly commercial production in large sheets/plates/tubes/pipes joining one similar or dissimilar metals on another, especially for the automotive industry and power plants. Explosive welding employed in this study can be used to join the AZ31 Mg and Al5005 alloys.
- Considering microstructural evaluation, a wavy interface formed between the AZ31 and Al5005 alloys after explosive welding. Adiabatic shear bands and equiaxed fine grains, including twin structures due to deformation, were observed on the AZ31 magnesium side near the interface.
- Metallographic observations showed that there was a sharp transition from the Mg side to the Al side and that intermetallic phases (such as Mg_2Al_3 and Mg_3Al_2) formed at the interface.
- It was found that there was both a sharp transition from two different metal sides to the other, as well as a transition with intermetallic phase formation, at the interface formed after explosive welding process. Experimental results and conducted detailed analyses showed a reasonable agreement with each other.
- According to mechanical characterization, the hardness of the AZ31 and Al5005 sides of the composite decreased to the original hardness away from the interface. Tensile test results showed that the explosively welded AZ31–Al5005 structure had an acceptable yield strength, tensile strength, and elongation. The toughness of the composite did not vary with temperatures.
- As expected, bimetallic corrosion occurred at the explosively welded interfaces. Heavy galvanic corrosion marks were also observed by SEM at the interfaces after the corrosion tests.
- The corrosion rate of the explosively welded structure increased owing to the high galvanic coupling between the Al5005 and AZ31 alloys.
- The corrosion behaviour of the AZ31–Al5005 composite in 3.5% NaCl was similar to that of AZ31. However, the corrosion potential of the explosively welded composite structure was nobler (+250 mV) compared to that of the AZ31 alloy.
- On the basis of the above discourses, this study's outcomes revealed that the interface characteristic was a critical effect on the microstructure, mechanical, and corrosion properties of end products, which still remains a blind spot in the available literature regarding explosively welded Al-Mg bimetallic composite systems.

Acknowledgements

Authors thank the MKE Barutsan Company (Turkey) for valuable contributions to the explosive welding process of the materials.

References

[1] M.D. Chadwick, J. Mech. Work. Technol. (1984), doi:10.1016/0378-3804(84)90133-5.
[2] M. Acarer, B. Gülenç, F. Findik, Mater. Des. (2003), doi:10.1016/S0261-3069(03)00066-9.
[3] J. Kaur, Int. J. Adv. Mater. Manuf. Charact. (2018), doi:10.11127/ijammc2018.09.02.
[4] A. Chiba, K. Hokamoto, M. Nishida, M. Fujita, Adv. Mater. 93 (1994), doi:10.1016/b978-0-444-81991-8.50171-0.
[5] R. Kaçar, M. Acarer, Mater. Sci. Eng. A (2003), doi:10.1016/S0921-5093(03)00643-9.
[6] R. Kacar, M. Acarer, J. Mater. Process. Technol. (2004), doi:10.1016/j.jmatprotec.2004.03.012.
[7] R. Mendes, J.B. Ribeiro, A. Loureiro, Mater. Des. (2013), doi:10.1016/j.matdes.2013.03.069.
[8] G.H.S.F.L. Carvalho, I. Galvão, R. Mendes, R.M. Leal, A. Loureiro, Mater. Charact. (2018), doi:10.1016/j.matchar.2018.06.005.
[9] M. Acarer, B. Demir, Mater. Lett. 62 (2008) 4158–4160, doi:10.1016/j.matlet.2008.05.060.
[10] H. Zhang, K.X. Jiao, J.L. Zhang, J. Liu, Mater. Des. (2018), doi:10.1016/j.matdes.2018.05.027.
[11] S.H. Ghaderi, A. Mori, K. Hokamoto, Mater. Trans. (2008), doi:10.2320/matertrans.MC200796.
[12] M.A. Habib, L.Q. Ruan, R. Kimura, P. Manikandan, K. Hokamoto, Mater. Sci. Forum (2013), doi:10.4028/www.scientific.net/MSF.767.160.

[13] S.H. Ghaderi, A. Mori, K. Hokamoto, Mater. Sci. Forum (2008), doi:10.4028/www.scientific.net/msf.566.291.
[14] F. Mahi, U. Dilthey, Ref. Modul. Mater. Sci. Mater. Eng. (2016), doi:10.1016/b978-0-12-803581-8.03785-1.
[15] Y. Kaya, Metals 8 (2018) Baseldoi, doi:10.3390/met8070544.
[16] D. Pronichev, L. Gurevich, M. Trunov, V. Yastrebov, Contemp. Eng. Sci. 8 (2015) 1083–1090, doi:10.12988/ces.2015.58241.
[17] O.I. Steklov, T.S. Esiev, N.K.A. Al-Sahib, Weld. Int. 15 (2001) 475–480, doi:10.1080/09507110109549390.
[18] P. Jonnard, K. Le Guen, R. Gauvin, J.F.Le Berre, Microsc. Microanal. 15 (2009) 36–45, doi:10.1017/S1431927609090060.
[19] M.A. Mofid, E. Loryaei, M.H. Heidary, J. Weld. Join. 37 (2019) 591–598, doi:10.5781/JWJ.2019.37.6.9.
[20] M. Wachowski, R. Kosturek, L. Śnieżek, S. Mróz, A. Stefanik, P. Szota, Materials 13 (2020) 1930 Baseldoi, doi:10.3390/ma13081930.
[21] H. Paul, J. Morgiel, T. Baudin, F. Brisset, M. Prażmowski, M. Miszczyk, Arch. Metall. Mater. 59 (2014) 1129–1136, doi:10.2478/amm-2014-0197.
[22] M. Nishida, A. Chiba, Y. Honda, J. Hirazumi, K. Horikiri, ISIJ Int. 35 (1995) 217–219, doi:10.2355/isijinternational.35.217.
[23] F. Kabakci, Enhancement Of Weld Metal Microstructure And Mechanical Properties With Ni/Co Addition On Electrode Cover For T/P92 Steels, Selcuk University, 2017.
[24] Y. Say, O. Guler, B. Dikici, Mater. Sci. Eng. A 798 (2020) 139636, doi:10.1016/j.msea.2020.139636.
[25] O. Guler, Y. Say, B. Dikici, J. Compos. Mater. 54 (2020) 4473–4485, doi:10.1177/0021998320933345.
[26] A. Pardo, M.C. Merino, A.E. Coy, R. Arrabal, F. Viejo, E. Matykina, Corros. Sci. 50 (2008) 823–834, doi:10.1016/j.corsci.2007.11.005.
[27] M.G. Acharya, A.N. Shetty, J. Magnes. Alloy. 7 (2019) 98–112, doi:10.1016/j.jma.2018.09.003.
[28] Q. Qu, J. Ma, L. Wang, L. Li, W. Bai, Z. Ding, Corros. Sci. 53 (2011) 1186–1193, doi:10.1016/j.corsci.2010.12.014.